JACS
JOURNAL OF THE AMERICAN CHEMICAL SOCIETY
Article
pubs.acs.org/JACS

The Reaction Mechanism with Free Energy Barriers for Electrochemical Dihydrogen Evolution on MoS_2

Yufeng Huang,[†,‡] Robert J. Nielsen,*[,†,‡] William A. Goddard, III,*[,†,‡] and Manuel P. Soriaga[‡,§]

[†]Division of Chemistry and Chemical Engineering, [‡]Joint Center for Artificial Photosynthesis, California Institute of Technology, Pasadena, California 91125, United States

[§]Department of Chemistry, Texas A & M University, College Station, Texas 77843, United States

Supporting Information

ABSTRACT: We report density functional theory (M06L) calculations including Poisson−Boltzmann solvation to determine the reaction pathways and barriers for the hydrogen evolution reaction (HER) on MoS_2, using both a periodic two-dimensional slab and a $Mo_{10}S_{21}$ cluster model. We find that the HER mechanism involves protonation of the electron rich molybdenum hydride site (Volmer−Heyrovsky mechanism), leading to a calculated free energy barrier of 17.9 kcal/mol, in good agreement with the barrier of 19.9 kcal/mol estimated from the experimental turnover frequency. Hydronium protonation of the hydride on the Mo site is 21.3 kcal/mol more favorable than protonation of the hydrogen on the S site because the electrons localized on the Mo−H bond are readily transferred to form dihydrogen with hydronium. We predict the Volmer−Tafel mechanism in which hydrogen atoms bound to molybdenum and sulfur sites recombine to form H_2 has a barrier of 22.6 kcal/mol. Starting with hydrogen atoms on adjacent sulfur atoms, the Volmer−Tafel mechanism goes instead through the M−H + S−H pathway. In discussions of metal chalcogenide HER catalysis, the S−H bond energy has been proposed as the critical parameter. However, we find that the sulfur−hydrogen species is not an important intermediate since the free energy of this species does not play a direct role in determining the effective activation barrier. Rather we suggest that the kinetic barrier should be used as a descriptor for reactivity, rather than the equilibrium thermodynamics. This is supported by the agreement between the calculated barrier and the experimental turnover frequency. These results suggest that to design a more reactive catalyst from edge exposed MoS_2, one should focus on lowering the reaction barrier between the metal hydride and a proton from the hydronium in solution.

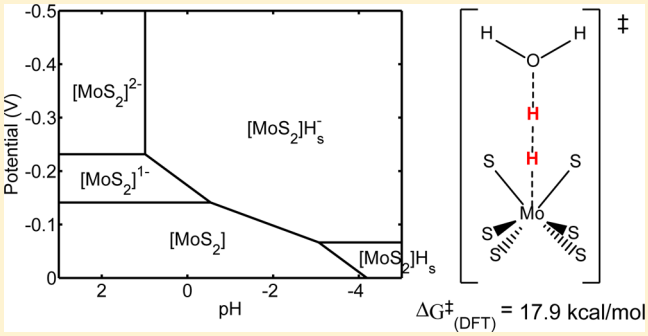

1. INTRODUCTION

A major challenge in renewable energy technology is water splitting, which is using solar radiation to photoelectrochemically convert water molecules into H_2 and O_2. Here both the hydrogen evolution reaction (HER) and the oxygen evolution reaction (OER) present challenges for the catalysts. The detailed reaction mechanisms have not yet been established for either one. Here we consider the easier case of HER.

Platinum is the most efficient inorganic HER catalyst; however, the cost of platinum has motivated an extensive search for earth abundant HER catalysts.[1] Hinnemann et al.[2] reported DFT calculations suggesting that molybdenum disulfide (MoS_2) can catalyze HER because of its nearly thermoneutral hydrogen adsorption energy. Indeed Jaramillo et al.[3] synthesized MoS_2 on Au(111) and showed that the activity for HER correlates linearly with the total length of the exposed edges of crystalline MoS_2. Since then, numerous experimental synthetic techniques have attempted to synthesize MoS_2 catalysts that carry out HER more efficiently.[4] Molecular analogues were also studied.[5]

Although the hydrogen adsorption energy has been a useful descriptor for screening materials to identify candidates for HER, it is reaction barriers that determine the rates. Thus, to design the most efficient HER catalysts, we must determine the reaction barriers for the various reaction sequences that can convert protons and electrons to H_2. Here the pathway with the lowest rate-determining step (RDS) is expected to dominate the reaction rate.

In this study, we perform density functional theory (DFT) quantum mechanics calculations to determine the reaction pathway for HER on the Mo-edge $(10\bar{1}0)$ of MoS_2. To enable the use of the most accurate DFT for reaction barriers while describing solvation effects at the Poisson−Boltzmann level, we describe the Mo-edge of MoS_2 using a $Mo_{10}S_{21}$ cluster model. This allows us to consider the introduction of protons and electrons separately and report free energies as a function of electrochemical potential and pH.

Received: March 30, 2015
Published: May 5, 2015

DOI: 10.1021/jacs.5b03329
J. Am. Chem. Soc. 2015, 137, 6692−6698

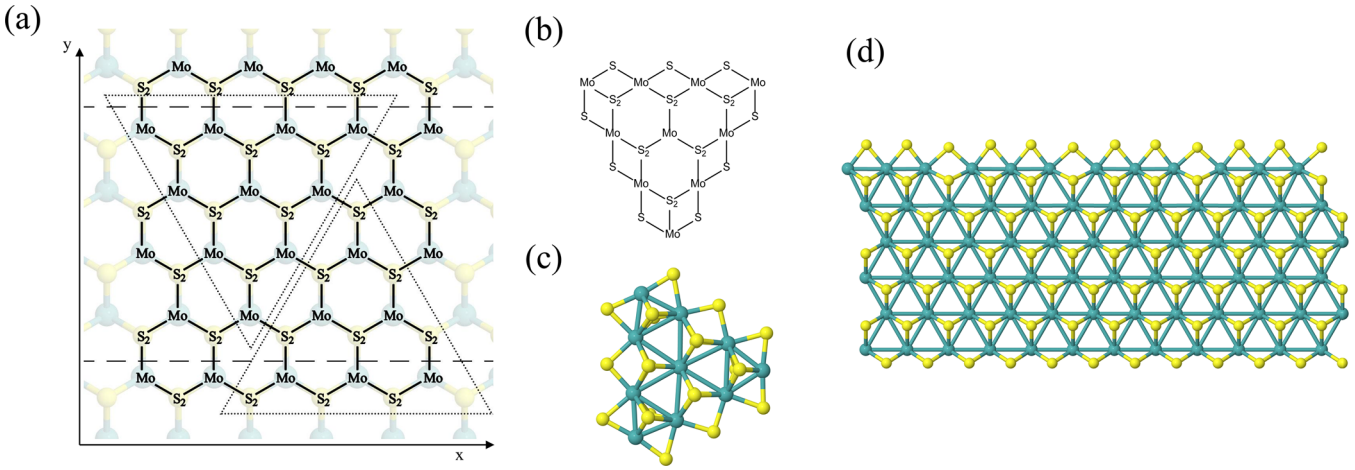

Figure 1. (a) Top view of the 2D MoS_2 sheet. The two horizontal dashed lines indicate terminations along the $(10\bar{1}0)$ Mo-edge and $(\bar{1}010)$ S-edge. The two triangles represent the terminations for Mo-edge and S-edge clusters; (b) Schematic representation of the 50% S coverage Mo-edge cluster; (c) Optimized triangular Mo-edge cluster with stoichiometry of $Mo_{10}S_{21}$. (d) Optimized structure of a 12Mo × 6Mo slab, where the Mo-edge (top edge) clusters into groups of 3 Mo. The same structure is obtained for the 3Mo and 6Mo wide slab.

2. COMPUTATIONAL METHODS

2.1. Finite Cluster. For the finite clusters we used the M06L[6] flavor of DFT, which has been found to give reliable energy barriers for reaction mechanisms of organometallic catalysts.[7] In these calculations we use the small core angular momentum projected effective core potential[8] from Hay and Wadt[9] to replace the inner 28 core electrons, so that 14 explicit electrons are described on each Mo (denoted LACVP**). All electrons are included for each S and H using the 6-31G** basis set[10] for structure optimization and the 6-311G**++ basis set[11,12] (hydrogen and oxygen) and the 6-311G-3df basis set[12,13] (sulfur) for the final electronic energy. The solvation energy was calculated by solving the Poisson−Boltzmann equation (PBF)[14] at the optimized geometry (using a solvent radius of 1.4 Å and a dielectric constant of 80.37). The vibrational frequencies used in obtaining the zero point energy, entropy, and enthalpy were calculated using the CPHF technique at the optimized geometry. All cluster calculations were performed with Jaguar.[15]

The free energy of an H_2 molecule at 1 atm and 298 K was calculated as above. The free energy of H^+ at 1 M in water (G = −270.3 kcal/mol) was taken to be its gas-phase value (G(H+, 1 atm) = H − TS = 2.5 k_BT − T × 26.04 = −6.3 kcal/mol) plus the empirical hydration energy (G(H+, 1 atm → 1M) = −264.0 kcal/mol).[16] Using the definition of the standard hydrogen electrode (SHE) condition where e^- and H^+ (pH = 0) are in equilibrium with 1 atm H_2, the free energy of an electron at SHE can be determined as the difference between the free energies of $1/2H_2$ and H^+. The chemical potential of electrons and protons away from SHE condition are then calculated as

$$\mu_e(E) = \mu_e(\mathrm{SHE}) - 23.06 \times E$$

and

$$\mu_H(\mathrm{pH}) = \mu_H(\mathrm{pH} = 0) - 1.36 \times \mathrm{pH}$$

both in kcal/mol. With these reference values, the free energies of the cluster with various numbers of electrons and protons can be compared.

2.2. Periodic Slab. For the periodic slab calculations we consider a single MoS_2 slab terminated on the $(10\bar{1}0)$ (Mo-edge) and $(\bar{1}010)$ (S-edge) boundaries with three Mo per unit cell as shown in Figure 1. Here we used the PBE[17] flavor of DFT with a plane wave basis set extending to 300 eV for geometry optimization and 500 eV for the final electronic energies. We used the projected augmented wave (PAW)[18] method for pseudopotentials to represent the effects of the inner 36 core electrons of Mo and the 10 electrons of the S, so that only the outmost 6 electrons of both Mo and S are described explicitly. Slab calculations are performed in VASP.[19]

Since the slab model consists of only a single S−Mo−S trilayer with both the Mo-edge and the S-edge exposed, we used the Monkhorst−Pack 4 × 1 × 1 k-point mesh, where 4 k-points are used in the periodic direction. The electronic energy was minimized within 0.1 meV, and the geometry was optimized to 0.1 meV/A.

For these periodic calculations the reference H_2 molecule is calculated in a 15A × 15A × 15A cubic vacuum space with only the Γ point.

3. MODEL SYSTEMS

3.1. Periodic Slab. The dominant phase for bulk crystalline MoS_2 is the 2H phase with AB stacking of the graphene-like hexagonal 2D sheets.[20] Upon synthesis, the exposed surfaces are generally the (001) basal plane of the S−Mo−S trilayer, the Mo-edge $(10\bar{1}0)$ and S-edge $(\bar{1}010)$. It was shown experimentally that the activity of the catalyst correlates directly with the total length of the exposed edges.[3] A recent experiment confirms this observation by comparing the activities between the edges and the basal plane.[21] In addition, we expect the chemistry of the edges of bulk MoS_2 to be similar to that of a single MoS_2 layer. It has been shown that additional layers decrease the current density due to electron hopping across the layers, such that the top layers are not as active as the bottom layers.[22] The exchange current density (0.6×10^{-7}A/cm^2)[22] reported for triangular pyramidal MoS_2 platelets is in the same order of magnitude as monolayer MoS_2 (1.3×10^{-7} A/cm^2).[3] The edges from the top layers contribute little to the activity, thus monolayer MoS_2 is sufficient to understand the chemistry of HER on MoS_2 edges.

STM studies of MoS_2 crystals show three stable edge configurations: 100% S coverage of the Mo-edge, 50% S coverage of the Mo-edge, and the S-edge.[23] Under the sulfiding conditions appropriate for hydrodesulfurization (HDS) processes the Mo-edge has been established experimentally as the dominant form; however, under HER conditions with no external sulfur the 50% S coverage of the Mo-edge is the most stable form.[24−26] This has also been observed in a recent HR-STEM study.[27] This structure was assumed in the previous DFT studies of HER on MoS_2.[2] Thus, to study HER electrocatalysis we chose to examine the 50% coverage case for the Mo-edge.

DOI: 10.1021/jacs.5b03329
J. Am. Chem. Soc. 2015, 137, 6692−6698

Experimental studies have observed finite MoS_2 clusters ranging from 1 nm to bulk. However, for systems of such large sizes, it is convenient to use periodic boundary conditions in the x direction, exposing the Mo-edge in the $+y$ direction and the S-edge in the $-y$ direction (Figure 1). We carried out DFT calculations for such periodic slabs and found that models that are three or six unit cells long in the periodic direction relax to structures 0.1 eV/Mo lower than models that are either two or four unit cells long. This has also been observed in other studies of the 50% S coverage Mo-edge calculations but not yet explained.[25,28]

This 3-Mo periodicity can be understood in terms of simple electron counting arguments. In the bulk the oxidation state of each Mo atom is +4 with bonds to 6 sulfur atoms, each of which bonds to 3 Mo. Thus, we can consider there to be 2/3 electrons from each Mo in each bond. In the valence bond description, this is described in terms of resonating structures. However, the surface stabilizes Mo−S valence bond structures with local 2-electron bonds. Thus, for the Mo terminated surface each edge sulfur contributes 1 electron to each Mo−S bond. Thus, each edge Mo contributes $2 \times 1 + 4 \times 2/3 = 14/3$ electrons to its six S neighbors. This implies that each triad of 3 Mo atoms on the edge contributes a total of 14 electrons for bonding. This would correspond to a d2 configuration on one Mo and a d1 configuration on the other two. Alternatively one can say that the full d2 band of the bulk system leads to a surface d2 band that is only 2/3 full. This leads to a Peierls distortion that has a periodicity of 3. Therefore, periodic calculations for slabs should always have a multiple of 3 edge Mo slab because it leads to an integer number of bonding electrons on the edge. In this reconstruction, three consecutive Mo atoms draw together (Mo−Mo distances of 2.96 A) leaving a larger separation (3.59A) between the triads. Indeed the calculations on an edge with 6 and 12 Mo periodicity in the x direction show the same triad reconstruction, as shown in Figure 1d.

3.2. Cluster Model. Using molecular clusters to model a periodic system for determining reaction mechanisms allows more flexibility in the accuracy of the methods (allowing us to use M06L which is more accurate for reaction barriers and bond energies than PBE,[7] the most common method for periodic calculations). It is straightforward to use clusters with net charges (difficult in PBC), and we can use the PBF (Poisson−Boltzmann) continuum solvation method that has been well-validated for aqueous solvation energies.[29] Indeed experiments can be carried out on supported MoS_2 to validate predictions.

Figure 1a shows how we extract a triangular cluster from the periodic array to expose only the Mo edges. Figure 1b shows the schematic representation of the finite cluster and Figure 1c shows the optimized structure.

3.3. Validation of the Cluster Model. To validate that the cluster model has the same chemical properties as the periodic Mo-edge, we calculated the binding energy of a hydrogen atom to both the cluster and the periodic slab, both under vacuum conditions. In both cases we reference the free H atom energy to that of 1/2 H_2 molecule. The results in Figure 2 show that the bond energies calculated using the cluster and slab models differ by 0.03, 0.06, 0.01, and 0.03 eV for the four stoichiometries.

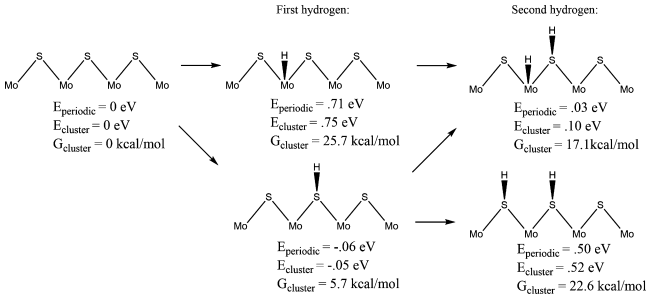

Figure 2. Hydrogen adsorption on the Mo-edge. $E_{periodic}$ is the relative electronic energy calculated from periodic calculations using 1/2 H_2 as the reference energy for H atom. $E_{cluster}$ is the relative electronic energy from cluster calculations, and $G_{cluster}$ is the relative free energy from cluster calculations. This indicates that the first H strongly prefers to bind to S by 0.8 eV, but the second H prefers to bind to a Mo instead of binding to a second S by 0.42 eV.

4. RESULTS AND DISCUSSION

We next describe the predicted energetics for the various reaction steps relevant for HER. Using the cluster model we can now add or subtract electrons and protons independently in discrete steps. First we calculate the free energies of the most likely intermediates to serve as a basis for describing the thermodynamics of HER. Then we examine the barriers of the various reaction steps to locate the rate limiting step.

4.1. Thermodynamics of the Mo-edge. Figure 2 shows that the first hydrogen strongly prefers to bind to the edge sulfur atom rather than the molybdenum atom by 0.8 eV (electronic energy) and leads to a net binding energy relative to H_2 of 0.05 eV. However, after including solvation effects, vibrational corrections, and entropy corrections, the free energy for adding a hydrogen atom to the edge S atom is 5.7 kcal/mol uphill relative to H_2.

Adding a second H to the Mo is only 11.4 kcal/mol uphill compared to 16.9 kcal/mol uphill for adding it to a second S. This disagrees with the previous assumption that the second H would go onto a second S,[2] but the Mo−H case was not calculated.

In order to evolve an H_2 molecule, protons and electrons must be added to the cluster. Here, it is useful to examine first the most stable structures with each number of extra electrons and each number of extra protons to understand the free energy differences between intermediate states, and ultimately find the lowest-barrier pathway. These free energies are shown in Figure 3.

1. At SHE conditions with E = 0 V and pH = 0, the most stable state is $[\mathbf{MoS_2}]$, the bare neutral Mo-edge.
2. The first reduction potential to obtain $[\mathbf{MoS_2}]^-$, is only −140 mV, leading to a negatively charged cluster solvated in water.
3. Protonating $[\mathbf{MoS_2}]$ leads to $[\mathbf{MoS_2}]\mathbf{H_S}^+$ (subscript S indicates the hydrogen atom is bound to a S atom) with an energy cost of 7.2 kcal/mol.
4. Instead of step 3, we can add a proton to the edge S having an extra electron, $[\mathbf{MoS_2}]^-$, to form $[\mathbf{MoS_2}]\mathbf{H_S}$, which costs ΔG = 2.4 kcal/mol, corresponding to a pK_A of −1.8. Comparing to $[\mathbf{MoS_2}]$ the cost of adding an H atom (a proton and an electron simultaneously) is ΔG = 5.7 kcal/mol as in Figure 2. If instead we put the H on the Mo to obtain $[\mathbf{MoS_2}]\mathbf{H_{Mo}}$ the energy is 25.7 kcal/

DOI: 10.1021/jacs.5b03329
J. Am. Chem. Soc. 2015, 137, 6692−6698

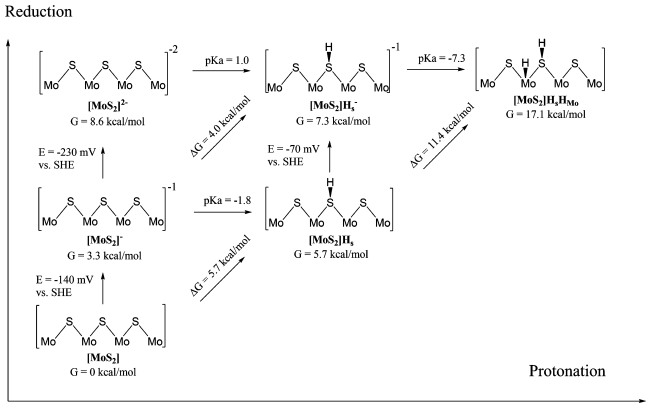

Figure 3. Thermodynamics (free energies at 298 K, pH = 0, and E = 0 V vs SHE) for the most stable configurations as a function of the number of protons and electrons added. Here we start with the Mo-edge cluster at equilibrium at the SHE potential. Each structure to the right has one additional proton. Each structure along the ordinate has one more electron, representing a reduction step.

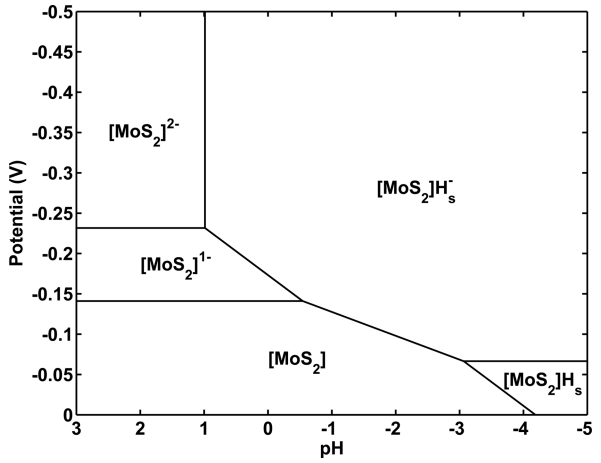

Figure 4. Calculated Pourbaix diagram for the surface states of the Mo-edge cluster.

mol relative to $[\mathbf{MoS_2}]$, corresponding to an excitation energy of ΔG = 20.0 kcal/mol.

5. Adding now an electron to $[\mathbf{MoS_2}]\mathbf{H_S}$ to form $[\mathbf{MoS_2}]\mathbf{H_S}^-$ occurs at a potential of −0.07 V. Moving the H from the S to the Mo, to form $[\mathbf{MoS_2}]\mathbf{H_{Mo}}^-$, costs ΔG = 5.9 kcal/mol.
6. Starting with $[\mathbf{MoS_2}]\mathbf{H_S}^-$ from step 5 we can add a proton to obtain $[\mathbf{MoS_2}]\mathbf{H_S H_{Mo}}$ at a cost of 9.7 kcal/mol (pK_A = −7.3).
7. Thus, the $[\mathbf{MoS_2}] \rightarrow [\mathbf{MoS_2}]^- \rightarrow [\mathbf{MoS_2}]\mathbf{H_S} \rightarrow [\mathbf{MoS_2}]\mathbf{H_{Mo}}^- \rightarrow [\mathbf{MoS_2}]\mathbf{H_S H_{Mo}}$ pathway may proceed with no highly endergonic steps.

We can also consider the case with more hydrogen on the cluster, which would be required by a Volmer−Tafel mechanism. However, as shown in Figure 3 an extra hydrogen is thermodynamically much more difficult, with a cost of about 11 kcal/mol ($[\mathbf{MoS_2}]\mathbf{H_s} \rightarrow [\mathbf{MoS_2}]\mathbf{H_S H_{Mo}}$).

On the basis of this thermochemistry, the highest-free energy intermediates for either a Heyrovsky ($[\mathbf{MoS_2}]\mathbf{H}^-$) or Tafel ($[\mathbf{MoS_2}]\mathbf{H_S H_{Mo}}$) mechanism are the last intermediates in the cycles. Therefore, we searched for rate-limiting transition states by considering the H−H bond forming steps, and then confirmed that the barriers connecting the preceding lower-energy intermediates are indeed lower.

4.2. Pourbaix Diagram. The intermediate species considered in Figure 3 lead to the Pourbaix diagram in Figure 4, showing the dominant phases as a function of pH and external potential. It is sufficient to use only the species in Figure 3, since only the most stable structure for a given stoichiometry appears on the Pourbaix diagram.

In the range of pH and potentials that are relevant to HER, 5 states are present. Starting from SHE at pH = 0 and E = 0 V, and applying increasingly negative potentials, the cluster is reduced first to $[\mathbf{MoS_2}]^-$ to become negatively charged. Further reducing the potential leads to the $[\mathbf{MoS_2}]\mathbf{H_s}^-$ structure (at pH = 0) rather than the −2 charged state. At very negative pH and potential, the $[\mathbf{MoS_2}]\mathbf{H_s}$ structure is the most favorable, since the potential is not sufficiently strong to further reduce the structure.

4.3. Transition States Analysis. Two types of transition states are considered in this study: the Volmer−Tafel mechanism in which two adsorbed hydrogens react to form H_2, and the Volmer−Heyrovsky mechanism with one adsorbed hydrogen reacting with a solvated proton. The calculated free energy barriers are shown in Figure 5, at a potential of 0 V and pH = 0.

4.3.1. Volmer−Tafel Mechanism. In the Volmer−Tafel mechanism, two adsorbed hydrogens next to each other react to form a dihydrogen molecule. Since there are two types of atoms, S and Mo, on the edge, we considered reactions of the type S−H + H−S and Mo−H + H−S. However, constraining the H atoms on two adjacent sulfurs to move toward a possible transition state, the hydrogen on one sulfur instead first moves onto the nearby Mo atom, forming a Mo−H species. Thus, a transition state of the type S−H + H−S is electronically unreasonable. Thus, the Volmer−Tafel reaction on the Mo-edge takes place between hydrogens on adjacent Mo and S atoms. Beginning from a relaxed geometry in which the H−H distance was constrained to 1.0 Å, eigenvector following was used to locate a transition state having a single imaginary frequency. This transition state geometry was found to have bond distances of 1.78 Å for Mo−H (compared to the equilibrium Mo−H bond of 1.67 Å), 1.08 Å for H−H (compared to a final H−H bond of 0.74 Å), and 1.56 Å for S−H (compared to a normal S−H bond of 1.35 Å).

The free energy at the transition state is 28.7 kcal/mol relative to the $[\mathbf{MoS_2}]$ ground state. It is 11.6 kcal/mol above the preceding intermediate $[\mathbf{MoS_2}]\mathbf{H_S H_{Mo}}$.

4.3.2. Volmer−Heyrovsky Mechanism. The Volmer−Heyrovsky mechanism is more complicated because it is necessary to solvate the H_3O^+ source of the proton along the reaction pathway. We find that to obtain accurate results requires the use of a cluster of 4 waters, one of which is protonated at the beginning but all of which are neutral at the end. However, in the reaction between an adsorbed hydrogen atom and the hydronium bound proton, the water cluster must rearrange to expose the proton for reaction.

First we examined the hydronium reacting with an adsorbed hydrogen atom bound to the edge sulfur atom. Again, transition state structures were located by following imaginary modes from constrained initial guesses. The transition state found for S−H + H−OH_2 has a free energy of 46.5 kcal/mol, which is too high for hydrogen evolution on the Mo-edge.

Using the same strategy, we found that the transition state free energies for reacting with the Mo hydrides $[\mathbf{MoS_2}]\mathbf{H_{Mo}}^-$ and $[\mathbf{MoS_2}]\mathbf{H_{Mo}H_S}$ are 26.7 and 23.6 kcal/mol. The barriers for

DOI: 10.1021/jacs.5b03329
J. Am. Chem. Soc. 2015, 137, 6692−6698

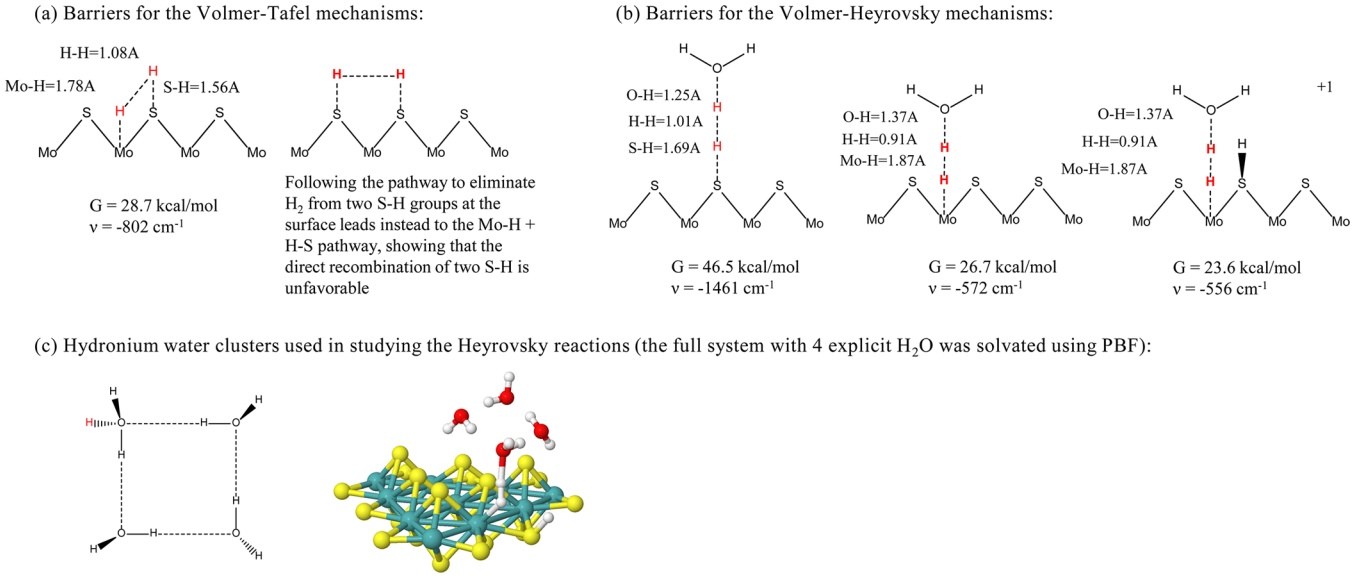

Figure 5. Schematics of the transition state structures considered for H_2 formation. Bond lengths and imaginary frequencies confirm transition state searches did not relax to products. The hydronium water cluster used for the Heyrovsky step is also shown. The red **H** indicates the reacting hydrogen atoms.

this process are much lower than the S−H case, making them the most favorable transition structures to form H_2. The free energy profile for these reactions shows that protonation of the edge S atom promotes hydride transfer, resulting in a lower barrier for hydride transfer from $[\mathbf{MoS_2}]\mathbf{H_{Mo}H_S}$ (G = 17.1 kcal/mol) than from $[\mathbf{MoS_2}]\mathbf{H_{Mo}}^-$ (G = 13.2 kcal/mol). The bond distances for the $[\mathbf{MoS_2}]$ case are 1.87 Å for Mo−H, 0.91 Å for H−H and 1.37 Å for H−OH_2, which correspond to a late transition state.

4.3.3. Overall Reaction. For the Mo−H + H−OH_2 transition state to be rate-limiting, we must confirm that the barriers in the previous steps are smaller. Choosing the $[\mathbf{MoS_2}] \rightarrow [\mathbf{MoS_2}]^- \rightarrow [\mathbf{MoS_2}]\mathbf{H_s} \rightarrow [\mathbf{MoS_2}]\mathbf{H_{Mo}}^- \rightarrow [\mathbf{MoS_2}]\mathbf{H_2}$ path described in the Thermodynamics of the Mo-edge section, we calculated transition states for the protonation and migration steps that are of smaller energy than the Heyrovsky barrier, as shown in Figure 6.

This mechanism gives insights on why MoS_2 is a good catalyst. The direct protonation of the Mo atom leads to a calculated high barrier of 28.1 kcal/mol, but in the presence of the S atom, the hydrogen adsorbs first on the chalcogenide, then migrates to the Mo atom (barrier = 20.5 kcal/mol), and finally reacts with a proton from solution to form H_2. These multiple steps lower the barrier for the whole process.

Toulhoat et al. computationally examined the dissociation of H_2 on MoS_2 edges in the context of hydrodesulfurization (i.e., water free).[30] In the absence of a protic solvent, our results are consistent that, among reaction mechanisms for the cleavage/formation of the H−H bond, the Tafel reaction of the type Mo−H + H−S provides the lowest energy pathway.

Finally, our result can be compared with estimates from Jaramillo's experimental study.[3] At a potential of −150 mV and pH = 0.24, he estimated a turnover frequency (TOF) of 1.64 × 10^{-2} s^{-1} per edge molybdenum atom for hydrogen evolution on the Mo edge clusters. Using transition state theory,

$$\text{rate} = (k_B T/h) \times \exp(-\Delta G^{\ddagger}/RT)$$

This TOF corresponds to a barrier of 19.9 kcal/mol. After adjusting our theoretical calculations for the chemical potentials due to the applied potential and pH, the ground state shifts to the negatively charged unprotonated structure, as shown in Figure 4. From the new resting state we calculate an adjusted barrier of 17.9 kcal/mol, very close to the 19.9 kcal/mol from the experimental estimate.

The Tafel slope b can also be estimated from the theoretical calculation, assuming electron transfer from the support to the catalyst does not limit the rate. We expect that $b = 2.3RT/nF \approx 60$ mV/n, where n is the difference in the number of electrons between the ground state and the transition state. Under reaction conditions, n = 1 since the ground state has shifted to the negatively charged structure, as shown in the Pourbaix diagram in Figure 4. In this case, the Tafel slope is 60 mV/dec, in agreement with the value of 55−60 mV/dec from the experimental Tafel plot.[3] Different polymorphs of MoS_2 have been shown to have different Tafel slopes, likely due to the effects of conductivity, which are minimized in the case of single MoS_2 layers on Au(111). For example, Chhowalla et al. measured a lower Tafel slope of 40 mV/dec using 1T-MoS_2, but proposed a different active site in the basal planes was responsible for HER.[31] Cao et al. also reported that the transition from crystalline MoS_2 to amorphous MoS_3 resulted in a change of Tafel slope from ca. 90 mV/dec to 40 mV/dec.[32]

■ CONCLUSION

Modeling the Mo-edge of a single MoS_2 sheet with a $Mo_{10}S_{21}$ cluster model, we found that the HER mechanism takes place through the Volmer−Heyrovsky mechanism involving an electron rich molybdenum hydride and a hydronium cation. This leads to an estimated barrier of 17.9 kcal/mol in good agreement with experiment, in which the barrier 19.9 kcal/mol is estimated from the turnover frequency (TOF).

We find hydronium protonation of the hydride on the Mo site is 21.3 kcal/mol more favorable than protonation of the hydrogen on the sulfur because the electrons localized on the Mo−H bond are readily transferred to form dihydrogen with hydronium.

The S−H + H−S Volmer−Tafel mechanism and the S−H + H−OH_2 Volmer−Heyrovsky mechanisms attempt to combine

DOI: 10.1021/jacs.5b03329
J. Am. Chem. Soc. 2015, 137, 6692−6698

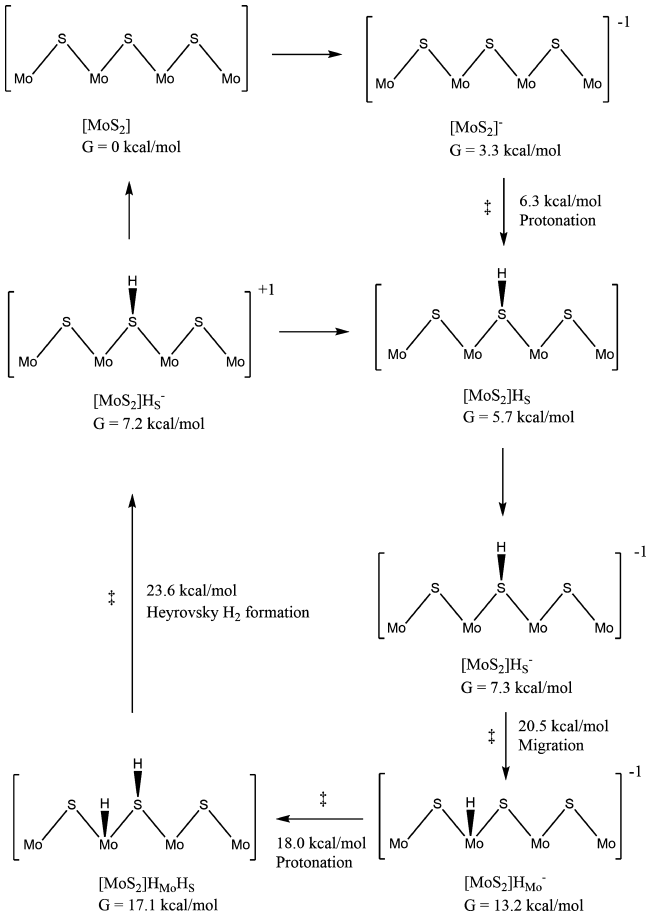

Figure 6. Overall reaction mechanism for HER on the Mo-edge cluster. The edge is first reduced by one electron, followed by a protonation to create a sulfur-bound hydrogen with a small barrier of 6.3 kcal/mol. The structure is further reduced by one more electron, followed by the migration of hydrogen onto the Mo atom with a relatively high barrier of 20.5 kcal/mol. The edge is protonated again by hydronium with a barrier of 18.0 kcal/mol. Finally, the metal hydride reacts with a proton from solution, forming dihydrogen with a barrier of 23.6 kcal/mol. All the free energies are relative to the ground state with no adsorbed hydrogens.

highly acidic hydrogen (i.e., two protons) to form H_2, leading to a higher barrier for transfer of electrons from the bulk. The Volmer–Tafel mechanism between molybdenum hydride and sulfur hydrogen has a relatively low barrier of 28.7 kcal/mol, for the same reason that electrons are easily transferred from hydride to form the hydrogen–hydrogen bond. Indeed, it is possible that tuning the pK_A of the edge chalcogenide could lower the barrier for this mechanism.

On the basis of the volcano plot concept,[33] it is widely believed that the binding energy of hydrogen on sulfur is the most important factor toward HER on crystalline MoS_2. However, we find that the sulfur–hydrogen species is not the critical intermediate since the free energy of this species does not play a role in determining the effective activation barrier.

In fact, we find that the predicted activation barrier for reaction between molybdenum hydride and hydronium is in agreement with the experimental rate of per-site TOF. This indicates that kinetic parameters should be used as a descriptor for reactivity, rather than equilibrium thermodynamics.

In conclusion, to design a more reactive catalyst from exposed MoS_2 edges, one should focus on lowering the reaction barrier between the metal hydride and a positively charged proton, either from the sulfur hydrogen species on the edge or from the hydronium in solution.

■ ASSOCIATED CONTENT

Supporting Information

Electronic energies and geometries of related compounds in the study. The Supporting Information is available free of charge on the ACS Publications website at DOI: 10.1021/jacs.5b03329.

■ AUTHOR INFORMATION

Corresponding Authors

*smith@wag.caltech.edu
*wag@wag.caltech.edu

Notes

The authors declare no competing financial interest.

■ ACKNOWLEDGMENTS

This material is based upon work performed by the Joint Center for Artificial Photosynthesis, a DOE Energy Innovation Hub, supported through the Office of Science of the U.S. Department of Energy under Award Number DE-SC0004993.

■ REFERENCES

(1) Laursen, A. B.; Kegnæs, S.; Dahl, S.; Chorkendorff, I. *Energy Environ. Sci.* **2012**, *5*, 5577–5591. Merki, D.; Hu, X. *Energy Environ. Sci.* **2011**, *4*, 3878–3888. Yang, J.; Shin, H. S. *J. Mater. Chem. A* **2014**, *2*, 5979–5985.

(2) Hinnemann, B.; Moses, P. G.; Bonde, J.; Jørgensen, K. P.; Nielsen, J. H.; Horch, S.; Chorkendorff, I.; Nørskov, J. K. *J. Am. Chem. Soc.* **2005**, *127* (15), 5308–5309.

(3) Jaramillo, T. F.; Jørgensen, K. P.; Bonde, J.; Nielsen, J. H.; Horch, S.; Chorkendorff, I. *Science* **2007**, *317* (5834), 100–102.

(4) Kibsgaard, J.; Chen, Z.; Reinecke, N.; Jaramillo, T. F. *Nat. Mater.* **2012**, *11*, 963–969. Li, Y.; Wang, H.; Xie, L.; Liang, Y.; Hong, G.; Dai, H. *J. Am. Chem. Soc.* **2011**, *133* (19), 7296–7299. Liao, L.; Zhu, J.; Bian, X.; Zhu, L.; Scanlon, M. D.; Girault, H. H.; Liu, B. *Adv. Funct. Mater.* **2013**, *23*, 5326–5333. Bonde, J.; Moses, P. G.; Jaramillo, T. F.; Nørskov, J. K.; Chorkendorff, I. *Faraday Discuss.* **2008**, *140*, 219–231. Merki, D.; Vrubel, H.; Rovelli, L.; Fierro, S.; Hu, X. *Chem. Sci.* **2012**, *3*, 2515.

(5) Appel, A. M.; Lee, S.-J.; Franz, J. A.; DuBois, D. L.; DuBois, M. R. *J. Am. Chem. Soc.* **2009**, *131*, 5224–5232. Karunadasa, H. I.; Montalvo, E.; Sun, Y.; Majda, M.; Long, J. R.; Chang, C. J. *Science* **2012**, *335*, 698.

(6) Zhao, Y.; Truhlar, D. G. *J. Chem. Phys.* **2006**, *125*, 194101.

(7) Zhao, Y.; Truhlar, D. G. *Theor. Chem. Acc.* **2008**, *120*, 215–241.

(8) Melius, C. F.; Olafson, D. B.; Goddard, W. A., III. *Chem. Phys. Lett.* **1974**, *28*, 457–462. Melius, C. F.; Goddard, W. A., III. *Phys. Rev. A: At., Mol., Opt. Phys.* **1974**, *10*, 1528.

(9) Hay, P. J.; Wadt, W. R. *J. Chem. Phys.* **1985**, *82*, 270. Wadt, W. R.; Hay, P. J. *J. Chem. Phys.* **1985**, *82*, 284.

(10) Hehre, W. J.; Ditchfield, R.; Pople, J. A. *J. Chem. Phys.* **1972**, *56*, 2257. Francl, M. M.; Pietro, W. J.; Hehre, W. J.; Binkley, J. S.; Gordon, M. S.; DeFrees, D. J.; Pople, J. A. *J. Chem. Phys.* **1982**, *77*, 3654. Hariharan, P. C.; Pople, J. A. *Theor. Chim. Acta* **1973**, *28*, 213–222.

(11) Krishnan, R.; Binkley, J. S.; Seeger, R.; Pople, J. A. *J. Chem. Phys.* **1980**, *72*, 650.

(12) Clark, T.; Chandrasekhar, J.; Spitznagel, G. W.; Schleyer, P. V. R. *J. Comput. Chem.* **1983**, *4*, 294–301.

(13) McLean, A. D.; Chandler, G. S. *J. Chem. Phys.* **1980**, *72*, 5639. Frisch, M. J.; Pople, J. A.; Binkley, J. S. *J. Chem. Phys.* **1984**, *80*, 3265.

(14) Tannor, D. J.; AMarten, B.; Murphy, R.; Friesner, R. A.; Sitkoff, D.; Nicholls, A.; Honig, B.; Ringnalda, M.; Goddard, W. A., III. *J. Am. Chem. Soc.* **1994**, *116*, 11875–11882.

DOI: 10.1021/jacs.5b03329
J. Am. Chem. Soc. 2015, 137, 6692–6698

(15) Bochevarov, A. D.; Harder, E.; Hughes, T. F.; Greenwood, J. R.; Braden, D. A.; Philipp, D. M.; Rinaldo, D.; Halls, M. D.; Zhang, J.; Friesner, R. A. *Int. J. Quantum Chem.* **2013**, *113*, 2110−2142.
(16) Tissandier, M. D.; Cowen, K. A.; Feng, W. Y.; Gundlach, E.; Cohen, M. H.; Earhart, A. D.; Coe, J. V.; Tuttle, T. R., Jr. *J. Phys. Chem. A* **1998**, *102*, 7787−7794.
(17) Perdew, J. P.; Burke, K.; Ernzerhof, M. *Phys. Rev. Lett.* **1996**, *77*, 3865. Perdew, J. P.; Burke, K.; Ernzerhof, M. *Phys. Rev. Lett.* **1997**, *78*, 1396.
(18) Blöchl, P. E. *Phys. Rev. B: Condens. Matter Mater. Phys.* **1995**, *50*, 17953. Kresse, G.; Joubert, D. *Phys. Rev. B: Condens. Matter Mater. Phys.* **1999**, *59*, 1758.
(19) Kresse, G.; Hafner, J. *Phys. Rev. B: Condens. Matter Mater. Phys.* **1993**, *47*, 558. Kresse, G.; Hafner, J. *Phys. Rev. B: Condens. Matter Mater. Phys.* **1994**, *49*, 14351. Kresse, G.; Furthmüller. *J. Comput. Mater. Sci.* **1996**, *6*, 15. Kresse, G.; Furthmüller, J. *Phys. Rev. B: Condens. Matter Mater. Phys.* **1996**, *54*, 11169.
(20) Wang, Q. H.; Kalantar-Zadeh, K.; Kis, A.; Coleman, J. N.; Strano, M. S. *Nat. Nanotechnol.* **2012**, *7*, 699−712.
(21) Wang, H.; Zhang, Q.; Yao, H.; Liang, Z.; Lee, H.-W.; Hsu, P.-C.; Zheng, G.; Cui, Y. *Nano Lett.* **2014**, *14*, 7138−7144.
(22) Yu, Y.; Huang, S.-Y.; Li, Y.; Steinmann, S. N.; Yang, W.; Cao, L. *Nano Lett.* **2014**, *14* (2), 553−558.
(23) Helveg, S.; Lauritsen, J. V.; Laegsgaard, E.; Stensgaard, I.; Nørskov, J. K.; Clausen, B. S.; Topsøe, H.; Besenbacher, F. *Phys. Rev. Lett.* **2000**, *84*, 951−954.
(24) Lauristen, J. V.; Bollinger, M. V.; Laegsgaard, E.; Jacobsen, K. W.; Nørskov, J. K.; Clausen, B. S.; Topsøe, H.; Besenbacher, F. *J. Catal.* **2004**, *221*, 510−522.
(25) Schweiger, H.; Raybaud, R.; Kresse, G.; Toulhoat, H. *J. Catal.* **2002**, *207*, 76−87.
(26) Moses, P. G.; Hinnemann, B.; Topsøe, H.; Nørskov, J. K. *J. Catal.* **2007**, *248*, 188−203.
(27) Hansen, L. P.; Ramasse, Q. M.; Kisielowski, C.; Brorson, M.; Johnson, E.; Topsøe, H.; Helveg, S. *Angew. Chem., Int. Ed.* **2011**, *50*, 10153−10156.
(28) Li, T.; Galli, G. *J. Phys. Chem. C* **2007**, *111*, 16192−16196.
(29) Jaramillo-Botero, A.; Nielsen, R.; Abrol, R.; Su, J.; Pascal, T.; Mueller, J.; Goddard, W. A., III. *Top. Curr. Chem.* **2012**, *307*, 1−42. Marenich, A. V.; Olson, R. M.; Kelley, C. P.; Cramer, C. J.; Truhlar, D. G. *J. Chem. Theory Comput.* **2007**, *3*, 2011−203.
(30) Prodhomme, P.-Y.; Raybaud, P.; Toulhoat, H. *J. Catal.* **2011**, *280*, 178−195.
(31) Voiry, D.; Salehi, M.; Silva, R.; Fujita, T.; Chen, M.; Asefa, T.; Shenoy, V. B.; Eda, G.; Chhowalla, M. *Nano Lett.* **2013**, *13* (12), 6222−6227.
(32) Li, P.; Yu, Y.; Huang, Y.; Nielsen, R. J.; Goddard, W. A., III; Li, Y.; Cao, L. *ACS Catal.* **2015**, *5*, 448−455.
(33) Nørskov, J. K.; Bligaard, T.; Logadottir, A.; Kitchin, J. R.; Chen, J. G.; Pandelov, S.; Stimming, U. *J. Electrochem. Soc.* **2005**, *152*, J23−26. Nørskov, J. K.; Bligaard, T.; Rossmeisl, J.; Christensen, C. H. *Nat. Chem.* **2009**, *1*, 37−46.

DOI: 10.1021/jacs.5b03329
J. Am. Chem. Soc. 2015, 137, 6692−6698